Comparison between the Light Harvesting Mechanisms of Type-I Photosynthetic Reaction Centers of Heliobacteria and Photosystem I: Pigment Site Energy Distribution and Exciton State

Akihiro Kimura,[*,†] Hirotaka Kitoh-Nishioka,[‡,¶] Yasuteru Shigeta,[¶] and Shigeru Itoh[†]

†*Department of Physics, Graduate School of Science, Nagoya University, Furo-cho, Chikusa-ku, Nagoya 464-8602, Japan*
‡*JST, PRESTO, 4-1-8 Honcho, Kawaguchi, Saitama 332-0012, Japan*
¶*Center for Computational Sciences, University of Tsukuba, 1-1-1 Tennodai, Tsukuba, Ibaraki 305-8571, Japan*

E-mail: akimura@tb.phys.nagoya-u.ac.jp
Phone: +81 52 789 2873. Fax: +81 52 789 2873

Abstract

The photosynthetic pigment system on the anoxygenic Type-I reaction center of Heliobacteria (hRC), which has a symmetrical structure, was analyzed. The excitonic coupling among all the bacteriochlorophyll *g* (BChl-*g*) molecules and chlorophyll *a* (Chl-*a*) molecules, and the site energy for each pigment were calculated by using Poisson-TrESP and the charge density coupling (CDC) methods. The obtained theoretical model reproduced the optical absorption and circular dichroism spectra. It also interpreted the decay associated spectra upon the photoselective laser excitation, which represent the ultrafast excitation energy migration process, better than the simpler hRC models that assumed constant pigment site energy shifts. Spatial movements of excitation energy on pigments on hRC upon the laser excitation were visualized. The energy dissipation by carotenoid molecules in hRC was also predicted. The hRC model was compared with the model of the reaction center of cyanobacterial photosystem I (PSI), which carries 95 Chl-*a* on the analogous Type-I structure with significantly different amino acid sequences, pigment species, and output redox powers. It is shown that the locations and site energy values of pigments in hRC resemble those in the core of PSI, except for the red Chl-*a* sites, suggesting common functional mechanisms implicated in their evolution.

INTRODUCTION

Natural photosynthesis converts solar energy into chemical energy to fix CO_2. The electronic excitation energy created by the absorption of a photon in one of the antenna pigments is promptly transferred to the central domain of the reaction center complex (RC), which includes a special pair of chlorophylls. Specific physical properties and arrangements of pigments on antenna/RC complexes seem to determine the efficiencies of excitation energy transfer (EET) and electron transfer (ET).[1] Experimental and theoretical studies on the elementary processes of RCs have been extensively performed to understand the optimization mechanisms under significantly different natural environments.[2–15]

Diverse pigment species, RCs and antenna-complexes, are used in photosynthetic organisms. Plants and cyanobacteria perform oxygen-evolving photosynthesis by using chlorophyll *a* (Chl-*a*) or Chl-*d* as the major pigment that absorbs visible blue and red light. In contrast, photosynthetic bacteria perform anoxygenic photosynthesis using bacteriochlorophylls (BChls), which mainly absorb far-red and blue light. Recent advances in the structural and theoretical/computational studies of RC/antenna complexes have opened new chances for the study of RC/antenna. In this study we have constructed *in-silico* models that contribute to new designs of natural/artificial photosynthesis.

In plant/cyanobacterial oxygenic photosynthesis, two types of RCs known as photosystems I and II (PSI and PSII) work in tandem. On the other hand, either a Type-I or a Type-II RC works in bacterial anoxygenic photosynthesis. In this study, we constructed a new theoretical model for Heliobacterial Type-I RC (hRC), whose fine structure was identified recently.[16] All Type-I RCs, including hRC, have similar architectures comprised of a peripheral antenna domain that binds 20-100 pigments and a central electron transfer domain that binds about 6 pigments to transfer electrons to a FeS cluster (F_X), and finally to NADPH. Different Type-I RCs absorb light at different wavelength ranges using different chlorophylls. The red-most absorption bands of pigments are at 700 nm (with a photon energy of 1.8 eV) for Chl-*a* in PSI, at 800 nm (1.5 eV) for BChl-*g* on hRC, and at 860 nm (1.4 eV) for BChl-*a* on green sulfur bacterial RC (gRC). All Type-I RCs use FeS clusters in contrast to Type-II RCs that use quinones as their terminal acceptors.[17,18] The structures of hRC[16] and gRC[19] are very unique among all the RCs being comprised of homodimers of only one protein species, expressed as $PshA_2$ and $PscA_2$, respectively. They are all assumed to have symmetrical structures.[20,21] This is in contrast to PSI, which is a heterodimer of two nearly homologous but different proteins viz. PsaA/PsaB. The structures of hRC and gRC contain 60

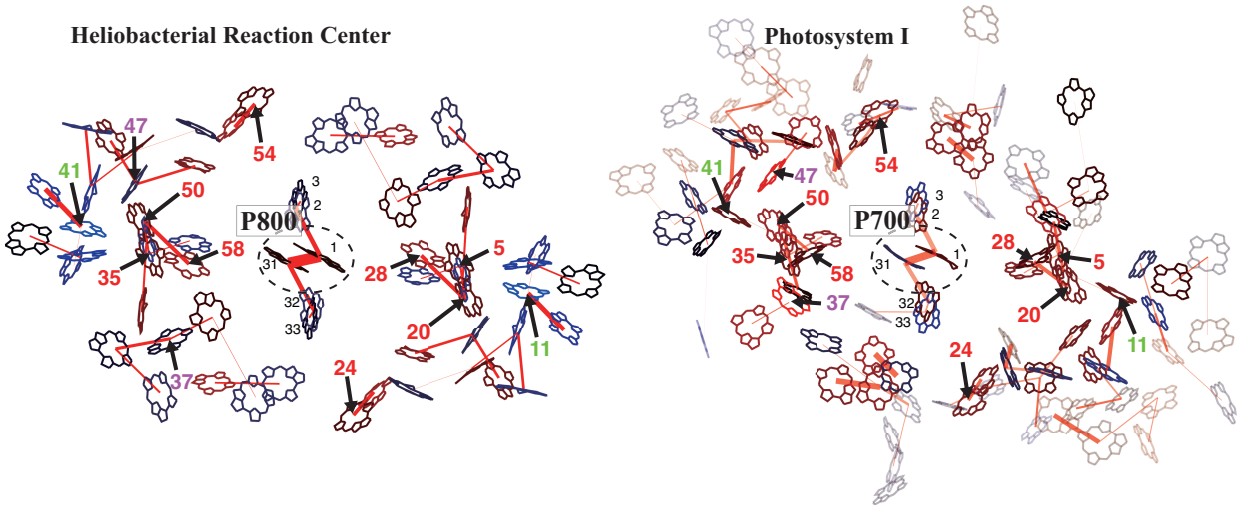

Figure 1: Arrangements and site energy shift of pigments in hRC[16] (left) and PSI[23] (right). Left: Arrangements of pigments (BChl-g, BChl-g', and Chl-$a_{\rm F}$) in hRC. The width of each red line shows the high probability of EET (square of excitonic coupling). Red/blue pigment colors represent the negative/positive shift of site energy. Right: Arrangements and site energy shift of pigments (Chl-a, and Chl-a') of PSI. Pigments drawn by opaque (transparent) pigments represent Chl-a that have (do not have) counterparts BChl-g on hRC. Carotenoid molecules contained in hRC and PSI are not shown (see Figure 3)

and 26 antenna bacteriochlorophylls, respectively. On the other hand, purple bacterial Type-II RCs contain only the electron transfer components surrounded by a ring of 18-22 BChls on LH1 antenna complexes.[18,22] PSII RC is made of two small proteins, which are homologous to the bacterial RC. The RC is surrounded by the two core antennas which bind 30 Chl-a and shows weak homologies to the peripheral regions of PSI RC proteins. The structures of RCs are diverse but are partially homologous to each other. Therefore, it is interesting to know the variation/optimization mechanisms of diverse RC/antenna structures theoretically through the construction of *in-silico* models.

The structure of hRC isolated from *Heliobacterium modesticaldum* provides locations of 54 BChl-g, 4 BChl-g',2 8^1-hydroxychlorophyll a (Chl-$a_{\rm F}$), 2 carotenoids, and FeS clusters on its symmetrical structure, as shown in Figure 1.[16] The locations of pigments in hRC overlaps with nearly 2/3 of the 95 Chl-a in PSI as shown in Figure 1. The hRC structure gives the precise locations of pigments in hRC; although it lacks two menaquinone molecules, which should function as electron acceptor (A_1) to mediate ET to F_X as shown by the EPR study.[11] We formed a simple theoretical model of the excitonic states of pigments in hRC based on this structure.[24,25] On the other hand, the difficulty of hRC purification historically limited the experimental studies on purified hRC. Thus, we referred to the works on isolated heliobacterial membranes, which are known to bind photosynthetic pigments only on hRC. Spectroscopic works on the membranes[26–32] have shown very fast EET dynamics suggesting the strong excitonic interaction among BChl-g in hRC, as predicted by our theoretical model.[24,25]

The absorption spectrum of hRC (see Figure 4), measured at cryogenic temperature, showed three BChl-g component bands at 778, 793, and 808 nm, and an absorption band of the special pair of BChl-g' P800. Transient absorption spectroscopy in the isolated membranes at room temperature[27,28] revealed very fast uphill EET to the shorter wavelength bands with a time constant (t_c) of 300 fs upon 812 nm excitation, and downhill EET with 100- and 500-fs-t_cs to the longer-wavelength bands upon 770 nm excitation. Similar fast EET was measured in the purified hRC,[13] which induced fast EET yielding in the higher excitation/charge separation at P800.[27] Single-molecule

spectroscopy by selective excitation at 670 nm of the Chl-a_F (A_0) in hRC has shown heterogenic function of A_0.[14]

Our simple excitonic model of hRC, based on the transition dipole approximation of BChl-g and constant site energy values at 785 nm for all the BChl-g molecules,[24] reproduced the fast EET process.[28] Numerical calculation of the exciton dynamics also reproduced the decay-associated spectra (DAS) obtained by laser spectroscopy. The estimated distribution of delocalized exciton states in hRC, suggested a stronger quantum coherence of hRC, was compared to that in PSI. It is indicated that the stronger transition-dipole moment of BChl-g molecule contributes to the stronger coherency and the faster energy transfer in hRC,[24,25] although the arrangement of BChl-g in hRC resembles that of Chl-a in the PSI. On the other hand, the PSI model with constant site energy values was unable to reproduce the absorption spectrum of PSI.[5]

Thus, we recently focused on the difference of pigment excitonic couplings in hRC and PSI. We modeled excitonic couplings in hRC by adopting the Poisson-TrESP method[8] that efficiently calculates the Coulomb interaction between pigments by using the transition ESP charges with Poisson equation, based on the TD-CAM-B3LYP.[25] The method yielded stronger excitonic coupling associations between the BChl-g molecules in hRC, compared to those between Chl-a in PSI. We also adopted the more exact method of Fragment Excitation Difference (FED) scheme[33] for the special pair P800, in which two pigments are very close to each other. The method gave a reliable interaction value of 234.2 cm^{-1} consistent with our previous estimation (250 cm^{-1}).[24] The excitonic couplings among BChl-g molecules in hRC was shown to be calculated even by simple dipole models except for the special pair.[25] On the other hand, the virtual replacement of BChl-g by Chl-a in hRC (or vice versa in PSI) indicated that both the different electronic structures of Chl-a and BChl-g, and the different pigment arrangements contribute to the differences between the hRC and PSI.[25]

In this study, we calculated the exciton model of hRC by calculating the site energy values for the first time, according to that of PSI by Adolphs et al.[8] The procedure is known to reproduce the absorption, circular dichroism (CD), and linear dichroism spectra of PSI with higher accuracy,[8] indicating the significance of site energy evaluation. We then analyzed the similarities/differences of the light-harvesting mechanisms of hRC and PSI comprehensively. The study predicted the locations of some BChl-g molecules that form energy sinks (low exciton states) in the EET from antenna BChl-g molecules to P800. The counterparts of such sink pigments are also shown to be conserved among the Chl-a molecules in PSI. On the other hand, hRC seems to have no counterpart sink sites for "PSI red-Chl-a".

We evaluated the site energy for each binding site of BChl-g in hRC by considering the effect of pigment environments, using the charge density coupling (CDC) method[8] (see Table 1) as described in the Theoretical Methods section. The newly calculated site energy values of hRC were compared with those on the PSI of a cyanobacterium *Thermocynecoccus elongatus*. We combined the results of our previous excitonic coupling study[25] with the site energy values, and calculated the optical spectra of hRC (Figure 4), the excitonic dynamics during EET and the DASs. The calculated absorption changes during the ultrafast EET upon the selective excitations of hRC almost reproduced the experimental ones measured at room temperature.[27] The functional, structural, and evolutionary relationships between the EET processes on the two Type-I RCs are discussed from a theoretical viewpoint.

THEORETICAL METHODS

Exciton Hamiltonian and CDC Method

We calculated the exciton states in hRC by solving the eigenvalue problem with $H_{\rm ex}$, as explained in the Supporting Information. We expressed the exciton Hamiltonian $H_{\rm ex}$ for hRC by

$$H_{\rm ex} = \sum_m E_m |m\rangle\langle m| + \sum_{m\neq n} V_{m,n} |m\rangle\langle n|, \tag{1}$$

where $|m\rangle$ represents the localized (first-)excited state of the mth pigment. The $V_{m,n}$, which represents the excitonic coupling between the mth–nth pigment pair, was taken from our previous results,[25] and was based on the FED method for the special pair, P800, and the Poisson-TrESP method for the other pigment-pairs. On the other hand, this study newly determined the site energy E_m in hRC using the CDC method. We denoted the excitation energy of mth pigment in a vacuum as E_0^m and, then, expressed the E_m by

$$E_m = E_0^m + \Delta E_m, \tag{2}$$

where ΔE_m represents a value of the site-energy shift from E_0^m caused by pigment-protein interactions in the RCs. In eq 2, we set E_0^m to 788 nm in the case that the mth pigment is BChl-g or BChl-g'. Since the 3th and 33th pigments in hRC are Chl-$a_{\rm F}$, we set E_0^3 and E_0^{33} to 670 nm. These E_0^m values were chosen to give best fits to the experimentally determined spectra of hRC and PSI, respectively, as described in the Results section. The CDC method approximates ΔE_m as[8]

$$\Delta E_m = \frac{1}{\epsilon_{\rm eff}} \sum_{J=1}^{K} \sum_{I=1}^{N} \frac{\Delta q_I^{(m)}}{|\mathbf{R}_I^{(m)} - \mathbf{R}_J^{(\rm bg)}|} q_J^{(\rm bg)}, \tag{3}$$

$$\Delta q_I^{(m)} = q_I^{(m)}(1,1) - q_I^{(m)}(0,0), \tag{4}$$

where $q_I^{(m)}(0,0)$ and $q_I^{(m)}(1,1)$ are the ground and the first-excited partial atomic charge on the Ith atom of the mth pigment, respectively. The $q_J^{(\rm bg)}$ represents the partial atomic charge of the Jth background atom. Note that we treated all atoms not belonging to the mth pigment as the background ones in eq 3. The $\mathbf{R}_I^{(m)}$ and $\mathbf{R}_J^{(\rm bg)}$ are the coordinates of the Ith atom of the mth pigment and the Jth background atom, respectively. In addition, it is noted that the effective dielectric constant $\epsilon_{\rm eff}$ is treated as a fitting parameter of 2.8 in hRC to reproduce the experimental results in eq 3 at 6 K. (See Refs. 8)

In the CDC calculations for hRC, we took into consideration all the molecules in the PDB data 5V8K except for Ca ions and dodecyl-maltosides (residue name LMT). We added the side chains of the missing amino-acid residues and hydrogen atoms to the structure determined by X-ray crystallography by assuming a standard protonation pattern for the titratable amino acid residues. The constructed system contains the PshA homodimer, 2 PshX subunits, 54 BChl-g, 4 BChl-g', 2 Chl-$a_{\rm F}$, 1 [4Fe-4S] cluster, 2 carotenoids (4,4′–diaponeurosporene, C4D), 4 phospholipids (DGG), and 477 crystal water molecules. We replaced the farnesyl group of BChl-g with a methyl group. The positions of the added hydrogen atoms were determined by the energy optimization at the MM (molecular mechanical) level of theory. Details of the system preparations are given in Supporting Information.

In this study, we also performed the pigment site-energy calculations on cyanobacterial PSI core complex from *Thermosynechococcus* (*T.*) *elongatus*, and compared them with the results from hRC. We prepared the PSI system of *T. elongatus* for the CDC method in a manner similar to that for

hRC. The details of the system preparation are also given in Supporting Information.

The $\{\Delta q_I^{(m)}\}$ for the target antenna pigment was evaluated by the restricted electrostatic potential (RESP) fitting scheme[34] to the charge densities of its ground and first excited state from the (TD-)CAM-B3LYP calculations. The $\{q_J^{(\mathrm{bg})}\}$ of the apo-protein parts and water molecules were set to those of AMBER *ff14SB*[35] and TIP3P,[36] respectively. On the other hand, the $\{q_J^{(\mathrm{bg})}\}$ of the other molecules were determined by using the RESP fitting scheme with the B3LYP/cc-pVDZ results. Tables S1 – S5 of Supporting Information list the resultant $\{q_I^{(m)}(0,0)\}$ and $\{q_I^{(m)}(1,1)\}$ for BChl-g, BChl-g', Chl-a_{F}, Chl-a, and Chl-a', respectively. The details of their derivations, in addition to $q_J^{(\mathrm{bg})}$, are given in Supporting Information.

Optical Spectra

The details of the theory used to calculate the optical spectra of hRC with H_{ex} (eq 1) are given in the Supporting Information. Here, we provide a brief explanation of their numerical conditions. We calculated the optical absorption, CD and DAS spectra of hRC using eqs S11, S12, and S20, respectively. We assumed the total Huang-Rhys factor to be one in eq S9. The density of the exciton states was calculated by eq S10 by assuming the Markovian limit in the observing transient absorption spectroscopy, since we only focused on the reaction rate in the light-harvesting process. We analyzed the exciton relaxation in hRC by the Redfield formula[37] because some exciton states are delocalized, as shown in the following section. The static disorder for the optical line shapes was modeled by a Gaussian distribution e^{-E^2/σ^2} with the HWHM (half-width at half maximum) σ of 120 cm^{-1} in order to provide the best fit around the long-wavelength region of the experimental spectrum at 6K. We used a σ value of 250 cm^{-1} as the temperature dependence for the static disorder for the calculation of the optical spectra at 300 K. The transition dipole moment, μ, of BChl-g was set to 6.5 debye.[38,39] We adopted the position $\boldsymbol{r}_m$ of the transition dipole moment of the mth pigment to the position of Mg in the PDB data list of hRC.[16] The direction of transition-dipole moment $\boldsymbol{\mu}_m/|\boldsymbol{\mu}_m|$ was defined from the distance vector between the positions of NB and ND atoms of BChls and Chl-a_{F} in the PDB data.

We analyzed energy transfer by calculating the DAS[40] obtained by using eq S20. Energy transfer processes between the exciton states were calculated according to the model after imaginal excitation of the system with either 770 nm laser pulse with a 30 fs HWHM or 812 nm laser pulse with a 60 fs HWHM to reproduce the experiments of the transient absorption spectroscopy performed at room temperature.[28] A temporal convolution of excitation pulse is not considered in the calculation of the transient difference spectrum and DAS because the spectral width σ_0 for the excitation pulse is included in the initial condition of eq S21 to solve the Redfield equation.

RESULTS

Site Energy Shifts

Values of site energy shifts of individual pigments in hRC (and PSI-core) were calculated as shown in Table 1, where pigment number $m(=1-30)$ is defined as the order of pigment in the PDB file of hRC (5V8K). The numbers of pigments in Table 1 show those defined in this study along with those defined in the PDB files of each RC. The pigment number $m(=31-60)$ corresponds to the C_2-symmetric $(m-30)$th counterpart. The $\Delta E_m^{\mathrm{hRC}}$ listed in Table 1 were calculated with the effective dielectric constant $\epsilon_{\mathrm{eff}} = 2.8$, which reproduced well the experimental optical absorption spectra, as shown in Figure 4. The PSI-core represents 57 Chl-a molecules (among total 96 Chl-a) on PSI, which are located at positions almost equivalent to those of BChl-g in hRC with respect

to the positions of the central Mg atoms (see Supporting Informationfor the numerical definition). Table 1 also lists the site-energy shifts, $\Delta E_m^{\mathrm{PSI}}$'s, calculated for the PSI-core. The $\epsilon_{\mathrm{eff}} = 1.5$ was used for their $\Delta E_m^{\mathrm{PSI}}$ calculations in accordance with Ref. 8. The red/blue color of each pigment in Figure 1 indicates the negative/positive value of site energy shift listed in Table 1.

We noticed that the values of site energy shift calculated by the CDC method did not show structural symmetry as seen in Table 1. The break in symmetry arises from the energy optimization process, wherein the number of hydrogen atoms that are not present in the PDB files are added.

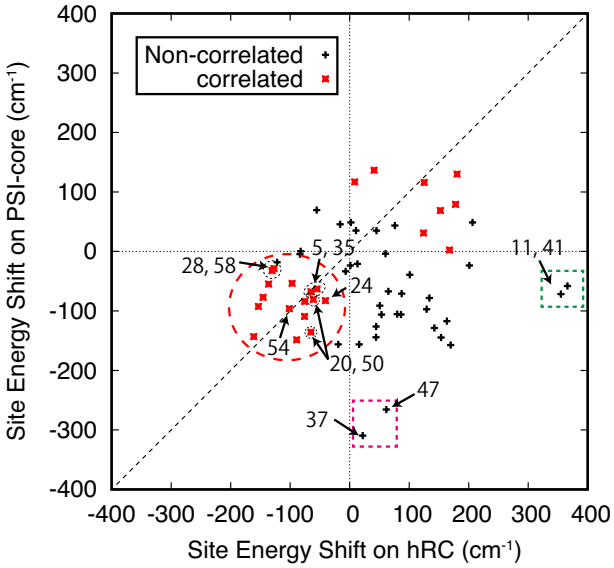

Figure 2: Relation between the site energy shifts of BChl-g in hRC and its counterpart Chl-a in the PSI-core. Numbers on some pigments are shown according to Table 1. Red marks represent the site energy shifts to the same positive (or negative) directions between each pigment in hRC and PSI. Green and magenta squares highlight the pigments with large site energy values of opposite signs between hRC and PSI.

We tested the relationship between the site energy shifts of Chl-a in the PSI-core and of their counterpart BChl-g in hRC (Figures 1 and 2). In Figure 2, the red points represent the pigment sites with positively correlated site energy shifts ($\Delta E_m^{\mathrm{hRC}}$, $\Delta E_m^{\mathrm{PSI}}$) and ($\Delta E_{m+30}^{\mathrm{hRC}}$, $\Delta E_{m+30}^{\mathrm{PSI}}$), where m is from 1 to 30. Among the red-colored points, the 5(35)th and 24(54)th pigments are close to the dotted straight line in Figure 2. The locations of these BChl-g in hRC and of their counterparts Chl-a in PSI-core are close to each other (situated almost at the homologous positions), as seen from Figure 1. We also plotted these site energy shift values with respect to the distance from special pairs P800 and P700 in Figures 3a and 3b, respectively. We defined the "distance" r_m as the distance of Mg of mth pigment from the center of two Mg atoms' of the two special pair pigments. The dependencies are apparently different for hRC and PSI-core. Results in Figures 2 and 3 will be discussed in more detail in the Discussion Section.

Exciton States

Exciton states formed by the pigments in hRC were calculated as described in Supporting Information by solving a Hamiltonian of eq 1, considering the site energy values obtained. Although the result was essentially similar to the one reported for the constant and homogeneous site energy models,[24] it gave better description of the exciton states in hRC, and reproduced the experimentally obtained absorption spectra, CD spectrum, and energy transfer dynamics in hRC well, as shown below.

Table 1: Site-energy shifts $\Delta E_m^{\rm hRC}$ ($\Delta E_m^{\rm PSI}$) cm^{-1} for individual pigments in hRC (PSI-core). The $\epsilon_{\rm eff}$ values are set to 2.8[a] (1.5[b]) for hRC (PSI-core) to provide a best fit to the experimental data. The rule of the pigment numbering m is explained in the text. m with an asterisk indicates the site energy shifts ($\Delta E_m^{\rm hRC}$, $\Delta E_m^{\rm PSI}$) and ($\Delta E_{m+30}^{\rm hRC}$, $\Delta E_{m+30}^{\rm PSI}$) with a positive correlation between each other.

m	Res#$^{\rm hRC}$	$\Delta E_m^{\rm hRC}$	Res#$^{\rm PSI}$	$\Delta E_m^{\rm PSI}$	m	Res#$^{\rm hRC}$	$\Delta E_m^{\rm hRC}$	Res#$^{\rm PSI}$	$\Delta E_m^{\rm PSI}$
1	1001	−6.7	1011	−33.4	31	1001	−16.0	1021	45.7
2	1002	87.3	1012	−71.0	32	1002	101.1	1022	−39.2
3*	1003	**8.4**	1013	**116.9**	33*	1003	**41.0**	1023	**136.5**
4	1004	133.9	1103	−78.2	34	1004	153.6	1202	−144.7
5*	1005	**−54.7**	1104	**−63.1**	35*	1005	**−65.0**	1203	**−67.7**
6	1006	13.0	1105	−20.8	36	1006	44.3	1204	−144.3
7	1007	16.1	1106	−156.1	37	1007	21.9	1205	−309.5
8	1008	201.0	1112	−23.6	38	1008	206.5	1211	48.9
9	1009	−82.4	1102	0.3	39	1009	−83.4	1201	−4.5
10*	1010	**152.4**	1108	**68.8**	40*	1010	**167.7**	1208	**2.4**
11	1011	354.9	1111	−71.6	41	1011	365.9	1210	−58.0
12*	1012	**180.5**	1110	**129.9**	42*	1012	**177.9**	1209	**79.1**
13	1013	1.1	1112	−23.6	43	1013	2.0	1211	48.9
14*	1014	**125.3**	1116	**116.0**	44*	1014	**124.2**	1214	**31.1**
15	1015	163.3	1117	−117.1	45	1015	169.6	1215	−157.3
16*	1016	**−75.7**	1119	**−83.9**	46*	1016	**−75.7**	1216	**−109.3**
17	1017	65.0	1123	−67.0	47	1017	61.6	1221	−265.6
18*	1018	**−96.7**	1122	**−53.6**	48*	1018	**−89.0**	1220	**−148.4**
19	1019	−55.4	1125	69.6	49	1019	−121.9	1223	−18.2
20*	1020	**−61.0**	1127	**−80.8**	50*	1020	**−65.3**	1225	**−135.6**
21	1021	129.3	1128	−97.2	51	1021	142.3	1226	−128.6
22	1022	79.8	1132	−105.4	52	1022	53.6	1230	−106.2
23	1023	45.0	1135	35.0	53	1023	44.4	1234	−126.1
24*	1024	**−40.8**	1136	**−82.6**	54*	1024	**−101.4**	1235	**−96.1**
25*	1025	**−145.4**	1137	**−77.1**	55*	1025	**−136.2**	1236	**−54.7**
26	1026	−19.2	1106	−156.1	56	1026	10.5	1206	35.0
27	1027	86.2	1138	−105.9	57	1027	76.0	1237	43.5
28*	1028	**−127.2**	1126	**−28.6**	58*	1028	**−130.5**	1224	**−32.3**
29	102	60.2	1302	−3.7	59	102	50.6	1207	−91.1
30*	103	**−153.3**	1139	**−92.5**	60*	103	**−161.3**	1238	**−143.1**

[a] The value is determined by the fitting procedure to reproduce the optical spectra of hRC with the CDC method (see the main body of text).
[b] The value is chosen in accordance with Ref. 8.

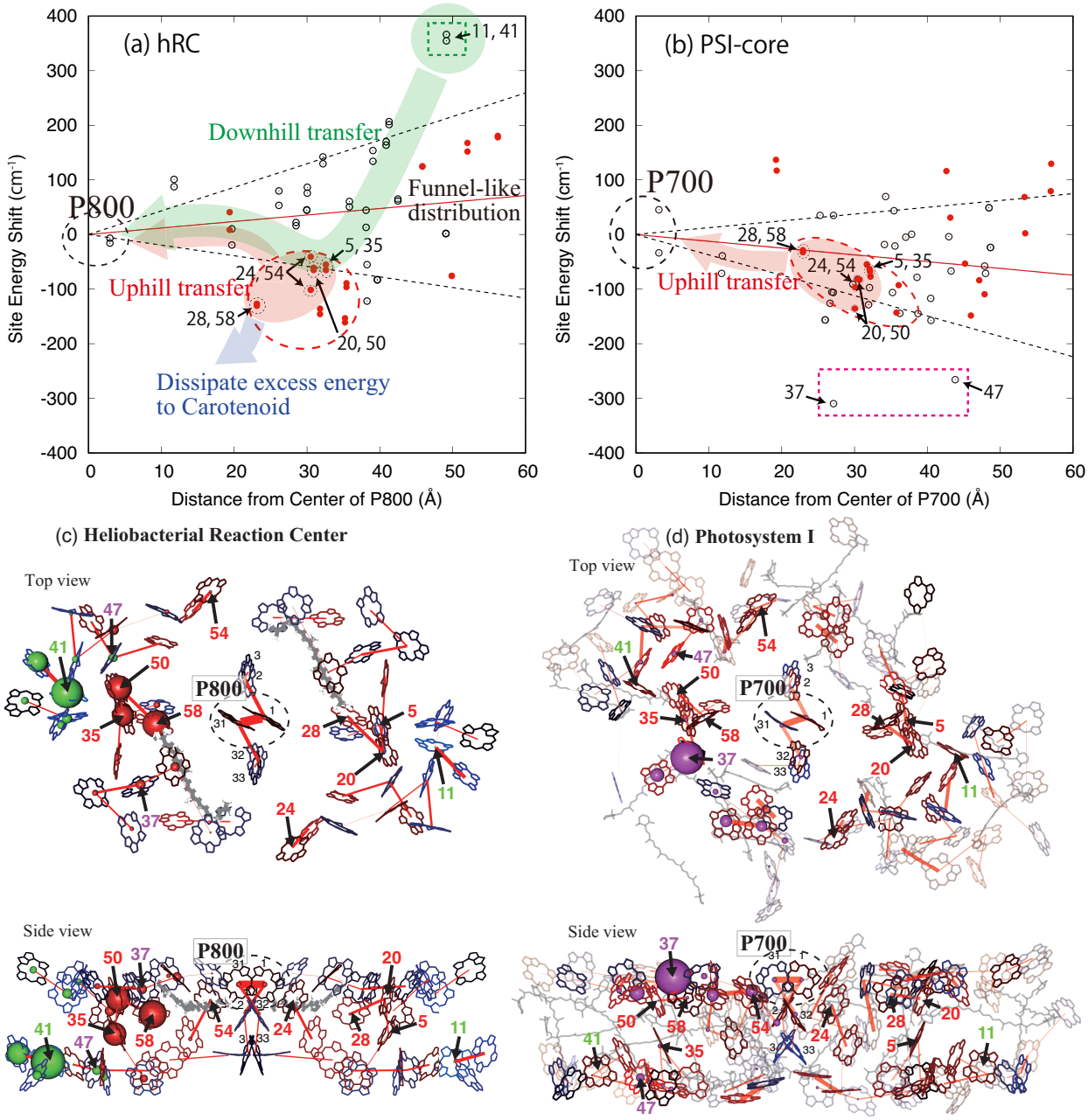

Figure 3: a) Site energy shift of BChl-g versus the distance from P800 in hRC. b) Site energy shift of Chl-a versus the distance from P700 in PSI-core. Broad green/red arrows represent the downhill/uphill EET processes. Solid and broken straight lines indicate the least-squares fitting line and standard deviations, respectively. The sites for pigments of special pairs P700, P800, putative "red-Chl-a" (37,47) and the other low energy pigments are also highlighted. c) and d) Probability of excitation of pigment in hRC and PSI. Arrangements of carotenoids[16,23] are also shown. The sizes of red and magenta spheres at the Mg atoms of the pigments represent the probabilities of excitation in the lowest exciton states in hRC and PSI, respectively. The green spheres on BChl-g represent those in the highest exciton state of hRC except for two excited Chl-a_{F}s. See movies in Supporting Information for the other exciton states.

We analyzed the spatial distribution of $|C_1^m|^2$ (namely, the excitation probability at the mth site in the lowest exciton state), where C_ν^m denotes the coefficient of the mth pigment site in the νth exciton state. The probability of being in the excited state $|C_1^m|^2$ of mth site in the lowest exciton state is shown as the sphere size at the central Mg atom of each pigment in Figure 1. The width of each red line that connects the Mg atoms represents the square of the excitonic coupling strength $|V_{m,n}|^2$. The widths are proportional to the probabilities of EET between m-th and n-th pigments. In the delocalized lowest excitonic state, the 28(58)th BChl-g was most excited, together with the 20(50)th and 5(35)th pigments.

We show the spatial distributions of $|C_\nu^m|^2$ for all exciton states as a movie files in Supporting Information. In the third lowest exciton state, the excitation probability was localized on the special pair P800, whose exciton energy was at about 806.5 nm, which is 6-nm red-shifted from the experimental value of 800 nm.

Optical Spectra

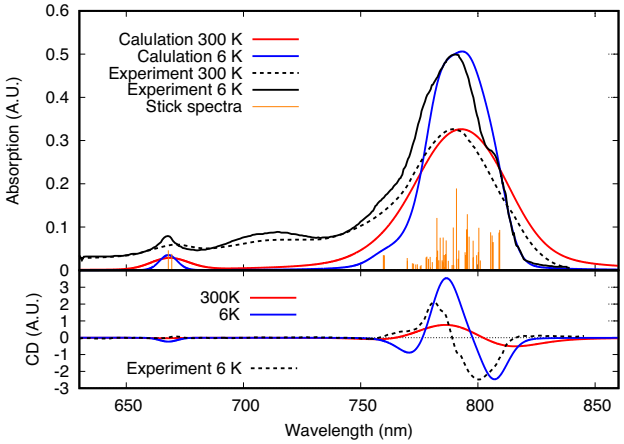

Figure 4: Top: Absorption spectra of hRC numerically calculated at 300 and 6 K with site energy values given in Table 1, and the spectrum experimentally obtained at 6 K. Stick lines show the numerically calculated line-absorption spectra. Bottom: Numerically calculated CD spectra of hRC at 300 and 6 K respectively. Details of the calculations are described in the section of optical spectra in the Results.

Figure 4 shows the absorption spectra of hRC calculated with eq S11 with parameters obtained in the present study. Within the CDC scheme,[8] we determined the fitting parameters (E_0, $\epsilon_{\rm eff}$, and σ) to reproduce the main peak and the width of the experimental spectrum, and the spectral shape in the lower energy side measured at 6 K. The values of $\epsilon_{\rm eff}$ were chosen as 1.5, 2.0, and 2.5 for PSI, CP29 and FMO, respectively.[8,41,42] We obtained the $\epsilon_{\rm eff}$ value of 2.8 for hRC, almost comparable to 2.5 estimated for the FMO protein,[42] to give the best fit to the long-wavelength edge of the 6-K experimental spectrum as shown in Figure 4. We also obtained the E_0^m of 788 nm for the BChl-g and BChl-g' sites, and 670 nm for the electron acceptor, A_0, Chl-a_F sites, respectively. The σ value was chosen as 120 cm^{-1} at 6 K, or 250 cm^{-1} at 300 K.

Figure 4 shows the numerically obtained CD spectra of hRC, which is calculated with eq S12. It yielded negative and positive peaks around 800 and 775 nm, respectively. The strength ratio of the two peaks was nearly one and showed no temperature dependency, in consistent with the experiment.[32]

Exciton Dynamics in hRC: DAS

The inverse of the participation ratio for each exciton state of eq S7 is shown in Figure 5. Degrees of delocalization of almost all the exciton states of hRC were larger than two, and smaller than those obtained with the previous simple exciton model.[24] However, there were still many delocalized exciton states, made of 16 pigments at the maximum. Hence, we analyzed exciton dynamics of hRC as the exciton relaxation processes by the Redfield formula of eq S8.

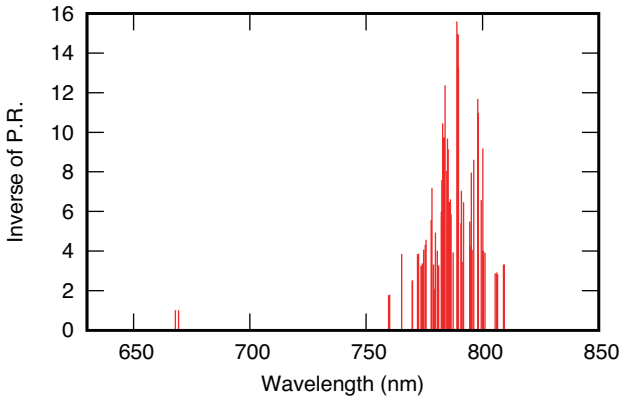

Figure 5: Inverse of participation ratio of the exciton states calculated in hRC

EET processes were simulated using the model as a transition between the exciton states during photoexcitation, with a laser pulse either at 770 nm of 30 fs HWHM or at 812 nm of 60 fs to reproduce the experiments performed at room temperature.[28] Figure 6 shows the analysis of EET processes using DAS,[40] calculated using eq S20. The negative/positive peaks in each DAS represent the energy efflux/influx at the given t_cs ($1/|R_\alpha|$ values).

All numerical results of the DAS analysis with different t_cs have been added to the Supporting Information. The amplitudes of DAS for large eigenvalues R_α (with very fast reaction t_cs in the sub-ps range) are almost negligible compared to those for small eigenvalues. Four DAS components with t_cs of 86 fs, 98 fs, 161 fs, and 1.4 ps resulted in non-negligible amplitudes with positive and negative peaks as shown in the Supporting Information.

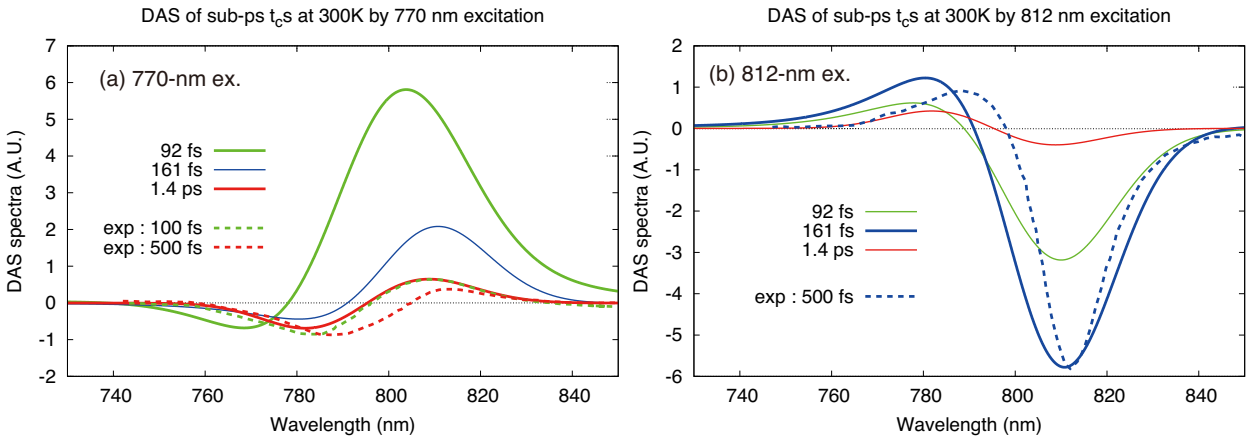

Figure 6: Numerical results of DAS analysis for some slower $t_c = 1/|R_\alpha|$, after photo-excitation with 770 (a) or 812 (b) nm pulse laser in hRC.

The t_c values of 86 fs and 98 fs are nearly equivalent so we combined these two DASs and compared as the average value of $(86+98)/2 = 92$ fs t_c with the experimental DASs in Figure 6. The negative peak strength of the DAS of 161 fs t_c is smaller than those of the other t_c values. Consequently,

upon 770-nm pulse excitation, it is necessary to obtain the dynamics represented by the double exponentials of 92 fs and 1.4 ps t_cs.

The peak strengths of 1.4 ps t_c upon the 812-nm pulse excitation are much smaller than those of the others in Figure 6b. The experimental 300 fs DAS upon the 812-nm pulse excitation was simulated with the 161 fs t_c component well. Hence, we used the 92 fs and 161 fs t_cs components for the numerical analysis of DAS.

Negative and positive peaks calculated for the 770 nm pulse excitation (Figure 6a) were seen at around 780 and 810 nm, respectively, and is consistent with the experimental peaks for 778, 793, and 808 nm showing the downhill EET. DAS, excited at 812 nm, showed 161 fs-t_c with positive and negative peaks (Figure 6b) at approximately 790 nm and 810 nm, respectively. The peaks at 790 and 810 nm agree with the experimental peaks at 793 and 808 nm, respectively, indicating uphill EET.[28]

DISCUSSION

We have theoretically analyzed the light-harvesting process in hRC, and compared them with those in PSI. The successful reproduction of absorption and DAS spectra using the simple exciton model in the previous study[24] inferred that the exciton model/state can be calculated rather well based on the transition dipole approximation by assuming the constant site energy values for all BChl-g in hRC. It indicated the significant contribution of the transition dipole moment of BChl-g that is larger than that of Chl-a. We further adopted the Poisson-TrESP method for the better calculation of the excitonic coupling strength between the pigments in hRC. It is found that the transition dipole approximation gave reasonable results for hRC (except for P800) but not for PSI. The feature came mainly from the different pigment molecular properties between BChl-g and Chl-a as well as the subtle differences of pigment arrangements between the hRC and the PSI. However, the spectrum with the narrower absorption band width should be obtained if we artificially assume the constant site energy values for all the BChl-g in hRC. We, thus, calculated the value of site energy shift for each pigment by considering the electrostatic interaction between the protein environments and the pigment, and combined it with the parameter set of the excitonic coupling strength using the Poisson-TrESP method in this study. This method enabled more quantitative analysis of the light-harvesting mechanisms on the two different RCs.

Optical Spectra

Figure 4 shows the absorption/CD spectra of hRC calculated by using the Poisson-TrESP and CDC methods. The results reproduced the experimental absorption/CD spectra qualitatively. It is also seen that the shoulder structure for the longer wavelength at low temperatures was reproduced better by the aforementioned simple model. Although the positions of the negative peaks of the calculated CD spectra were about 6 nm red-shifted from the experimental ones,[32] the discrepancy will be decreased by adjusting the parameter E_0^m. The exciton model also reproduces DAS for the case of the 770 or 812 nm excitation as shown in Figures 6a and 6b, respectively.

The width of the absorption spectrum, obtained by the P-TrESP method with constant values of site energy, is approximately 50% narrower than that obtained by the previous simple model.[24,25] We concluded that the simple model overestimated the delocalization of the excitonic states because the EET in the constant site energy model[24] is in a state of resonance. On the other hand, individual site energy shifts were given by the CDC method in this work by calculating the electrostatic environments around pigments. It suppresses the delocalization of the exciton state and lowers the energy level. More reliable shifts will affect the energy distributions on hRC, although more efforts

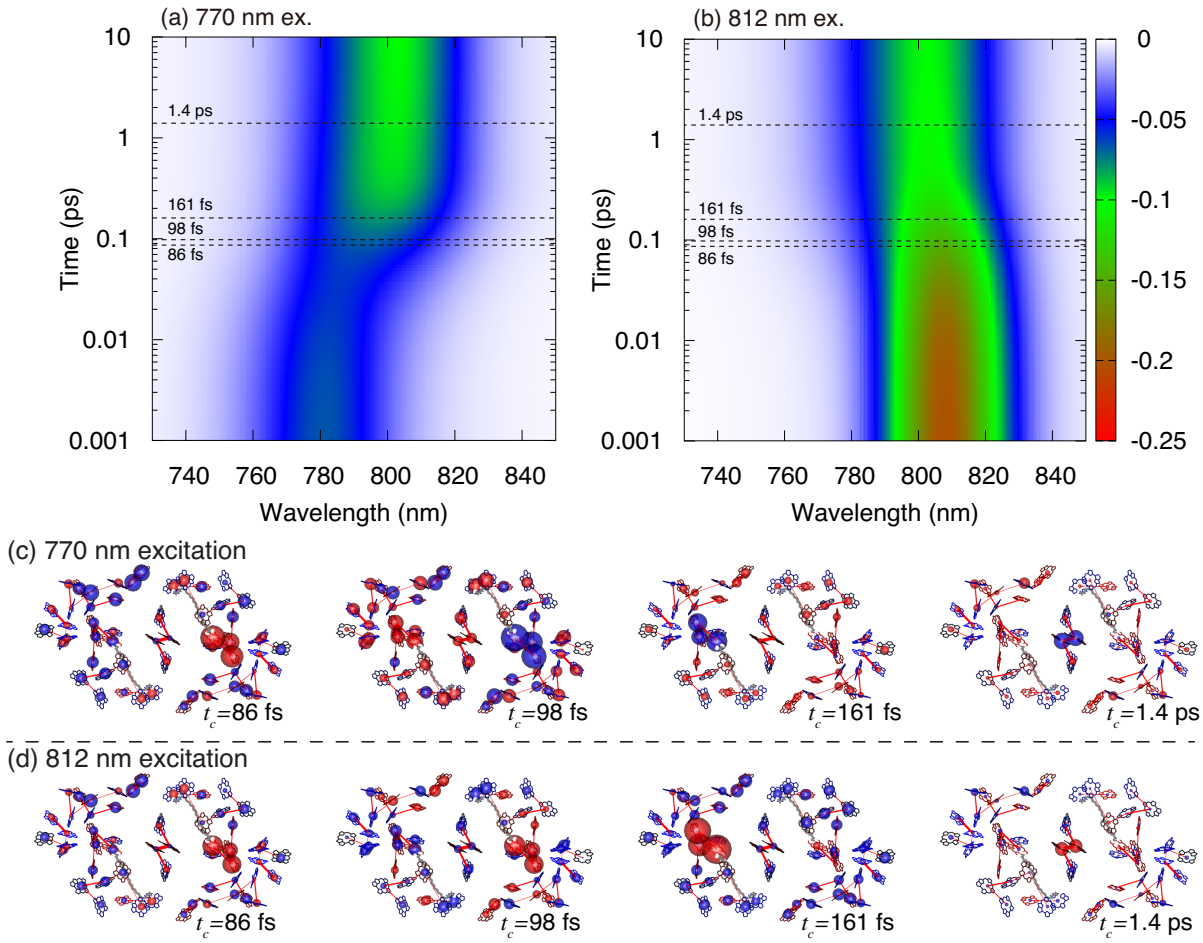

Figure 7: Upper panel: Numerical calculations for transient difference absorption spectrum $\Delta A(E,t)$ in hRC after 770 (a) or 812 (b) nm laser pulse excitations. Lower panel: Increase/decrease in excitation probability on each pigment after 770- (c) and 812-nm (d) excitations at different time constant (with different $t_c = 1/|R_\alpha|$). Difference excitation probabilities $\delta\rho_\alpha^m$ on each pigment calculated for the cases of DASs with four t_cs are shown. Sizes and colors of spheres on each m-th pigment express the absolute amplitudes of $\delta\rho_\alpha^m$, and the signs representing the increase (blue) and decrease (red) in the probabilities, respectively.

are required to improve this type of analysis.

The DAS analysis used in this study contributes to the investigation of hRC dynamics. The experimental t_cs of DAS were 100 and 500 fs during the downhill transfer upon the 770-nm excitation, and 300 fs during the uphill transfer upon the 812-nm excitation.[28] Thus, the t_cs for the downhill and uphill transfers were different from each other. In our previous study, we reproduced the DAS with t_cs of 71 and 139 fs upon excitation at 770 nm and with a t_c of 71 fs upon excitation at 812 nm.[24] However, the t_cs could not be decomposed into three, in contrast to the calculated result. On the other hand, this study suggested two t_c values of 92 fs and 1.4 ps for the downhill transfer and a t_c value of 161 fs for the uphill transfer. The same 71 fs t_c obtained in the downhill/uphill transfer in the previous study was split into two because of the inhomogeneity of the site energy values. Therefore, DAS analysis leads to a more reliable exciton model based on the reproducibility of the exciton dynamics.

The transient difference absorption spectra $\Delta A(E,t)$ induced by 770- and 812-nm excitation pulses were calculated as shown in Figure 7a and 7b using eq S19. The two spectra were different from each other within 0.1 ps after the excitations, and then converged into similar long-lived

spectra peaking at 803 nm after 1 ps. The long-lived spectra interpret the steady state fluorescence emission spectrum of hRC. The emission spectrum calculated at 6K with a peak at around 810 nm is also shown in supplementary Figure S6. We, thus, estimate that the downhill/uphill EETs on hRC that occur at 0.1-1 ps give variable $\Delta A(E,t)$ at 0.1-1 ps, which correspond to the distribution changes in specific exciton states. After this, the two processes exhibit almost similar difference spectra at the longer time range.

Images in the lower panel (Figure 7c and 7d) show the spatial expression of DAS showing variation of excitation probabilities on individual pigments with four t_c values (see dotted lines in Figure 7a and 7b) calculated by eq S22. The images provide an insight into the explicit variations of each component in the exciton states among BChl-g's on hRC. It is noted that the EETs with 86-fs t_c give similar difference spectra irrespective of the excitation wavelength. The EET is the uphill one, because the decrease in the excitation energy is prominent at the 5-, 20-, and 28-th BChl-gs in the second-lowest exciton state as shown in Supporting Information movie, and the increase in the peripheral pigments is larger than that in the lowest exciton state.

Specifically, amplitudes/distribution of excitation probabilities were very similar in the 86-fs-t_c EET after both the 770- and 812-nm excitations (Figure S4) suggesting similar EET mechanisms in the 86-fs-t_c DAS. Although the 5, 20, 28-th BChl-g's mainly contribute to the uphill EET for 86-fs-t_c DAS, the changes of excitation energy suggest this EET to be uphill from a sort of low-energy bottleneck state, which can be populated to similar extents either through the uphill EET after the 812-nm excitation or the downhill EET after the 770-nm excitation.

The signs of energy changes on pigments in all DAS, except for 86 fs-t_c's one, after the 770-nm excitation in Figure 7c are opposite to those after the 812-nm excitation in Figure 7d. The distribution with 98-fs-t_c after the 812-nm excitation in Figure 7d is similar to that with 86-fs-t_c showing uphill transfer. On the other hand, the signs of excitation change with 98-fs-t_c DAS after the 770-nm excitation are opposite to those with 86-fs-t_c, indicating the downhill nature. In the case with 161-fs-t_c, EET occurs between the lowest exciton state and the other exciton states, because the changes on the 35-, 50-, and 58-th BChl-gs are apparently prominent for the lowest exciton state (Figure 3c). Similarly, EET with 1.4-ps-t_c occurs between the third lowest and the other exciton states, because the changes on the two BChl-g molecules of the special pair are prominent in the third-lowest exciton state as shown in Supporting Information movie. The phase with 1.4-ps-t_c upon the 812-nm excitation in Figure 7d appears to reflect the EET without P800 that does not compete with the charge separation reaction.

The numerically obtained probabilities of excitation in the lowest exciton state are shown in Figure 1. The probabilities were distributed mostly among the 28(58)th, 20(50)th, and 5(35)th pigments, close to P800 at the inner side of the circular pigment arrangement in hRC. The distribution is basically similar to the one indicated in the simpler models that did not consider variation of site energy shifts.[24] Interestingly, the site energy shifts for these pigments constituting the lowest exciton state are mostly negative, and seem to stabilize it further. It is, therefore, suggested that the component pigments of the lowest exciton state play key roles for the uphill EET to P800, and should be critical for the following charge separation reaction on P800 too. Thus, we can assume that future modifications of these pigments or their environments by site directed mutations, or by some other means, will induce drastic changes in the EET of hRC.

The estimated pattern of excitation energy distribution on hRC is more localized compared to the constant site energy model.[24] The probability distributions shown in Figure 3 for all exciton states are presented in Supporting Information. The difference comes from the effects of inhomogeneous environments on the site energy shift of pigments.

Since the components of exponential decay were extracted using DAS analysis, we applied the Markov limit to the rate equation. However, we did not consider non-Markovian processes to analyze the molecular vibrations and exciton states that are coherently coupled to the exciton

dynamics occurring at rates shorter than sub-ps.

The hRC bears a large number of pigments on its complex protein structure, so we assumed $S = 1$. In the numerical analysis, using the Redfield formula at $S = 1$, we used the spectral density $J(\omega)$ of eq S9. It resulted in a reorganization energy of about 100 cm^{-1}.[43] On the other hand, a smaller reorganization energy, by three times, was estimated for the core complex of PSII.[6] If we assume a similar extent of reorganization energy, it should result in three-times smaller Redfield rate constant of exciton relaxation. Determination of the reorganization energy for the hRC is, therefore, necessary for the analysis of temperature dependence of the absorption spectra by considering the dynamic/static fluctuations as done for the FMO system.[44,45] Higher degrees of freedom for spectrum analysis as well as an extended numerical search for hRC/PSI that is significantly larger and more complex than FMO may lead to the optimization of models.

This study expanded our simple models,[24,25] which calculated only pigment-pigment interactions, to a more concrete and practical one. We have considered the physical properties of pigments as well as its interaction with protein environments in this study. We qualitatively reproduced the overall optical absorption, CD, and DAS, although a more quantitative consideration of dynamic/static fluctuations are still needed. It is interesting to understand how the potential barrier in the uphill EET, from the lowest exciton state to the special pair, can be overcome by thermal fluctuations.

In this paper, we have analyzed the exciton dynamics of hRC by using Redfield theory, namely by assuming delocalized exciton states of hRC. However, the analysis of the inverse of participation ratio in Figure 5 showed that the smallest size of quantum delocalization is about two. The size of the exciton delocalization will be smaller if we consider the dynamical disorder to the exciton dynamics in hRC. Then, the generalized Förster theory[46] will be required for EET analysis. The study of the density of exciton-phonon interactions in hRC by the molecular dynamics simulation is also a future task.

Site Energies

The spatial distribution of site energies in hRC are seen from Figure 1a. Site energy values of BChl-g, except for the 21(51)th BChl-g that are too close to P800, are lower than those of BChl-g far from P800. Especially, 28(58)th, 20(50)th, and 5(35)th pigments in the lowest exciton state are close to P800 as seen in Figure 1.

The slope of the fitted line in the distance dependencies of site energy shifts in hRC (solid line in Figure 3) was slightly positive, showing the large dispersion. Especially, the largest positive site energy shifts are seen for 11(41)th BChl-g located at about 50 Å from P800. Our exciton model for hRC, thus, apparently supports the idea of the funnel-like distribution of site energy, which assumes a more negative/positive shift at shorter/longer distance.[1]

Some pigments have the site energy values lower than that at 800 nm. The 28(58)th BChl-g has the largest probability of excitation among the pigments forming the lowest exciton state in Figure 1a. These pigments are close to the electron transfer chain composed of P800, A_{CC} and A_0, and will give excitation energy to P800 or to the pigments in the higher exciton state, as shown in Figure 6. Interestingly, two carotenoid molecules are located nearby the 28(58)th BChl-g (see Figure 1). They may, therefore, function as the energy sink and, if necessary, dissipate the excess excitation energy on the low exciton state. We will analyze the energy dissipation from BChl-g in these low energy sites to the carotenoids via the triplet state of BChl-g in the future.

The site energy shift of 28th BChl-g causes a red-shift of 210 cm^{-1}. It is induced by the interaction with the Lys (596A) residue. The data obtained by component decomposition of the site energy shift for hRC and PSI were added to Supporting Information. The residue exists deep inside the hRC, in contrast to the other Lys residues that exist closer to the membrane surface region. In PSI, on the other hand, all Lys residues exist near the membrane surface. We find no homologous Lys residue

on the amino acid sequences/structures of PSI and gRC proteins. On the other hand, the 28(58)th BChl-g, whose excitation probability in the lowest (second) exciton state is the largest, is located nearby Chl-a_{F} (A_0). The situation might be related to the recent results from single molecule spectroscopy on excited fluorescence of individual Chl-a_{F} from hRC, which have shown heterogenic function of A_0.[14] We assume that BChl-gs being excited under steady state after photoexcitation of Chl-a_{F} are located at the inner side of hRC.

Comparison with PSI

The different site energy shift patterns/values in hRC and PSI are expected to produce different exciton models/states, and consequently affect their absorption spectra. In the analysis, the value of effective dielectric constant ϵ_{eff} was introduced as an arbitrary parameter to obtain better fits of the peak position, width, and shape of the absorption spectrum to the experiments. Therefore, it is not appropriate to relate the different values of site energy shifts in hRC/PSI directly to the overall spectra. However, we noted that the site energy shifts are more negative in PSI with larger absolute values. The effect of different distributions of site energy shifts in hRC, then, can be evaluated critically from the effects on the exciton states at levels lower than those of the special pairs.

We compared the dependencies of the site energy values on the distance from P800 in hRC and from P700 in PSI. The values in PSI are mostly similar to, but a little different from, those reported by Adolphs et al.[8] We defined the PSI-core moiety which contains 57 Chl-a pigment, whose locations resemble those of BChl-g in hRC. The distance dependencies of site energy shifts in the PSI-core in Figure 3b suggest that the 37th and 47th Chl-a located at 25 and 45 Å from the center represent some red-shifted Chl-a with extremely low site energy values so that the distribution of site energies in PSI does not fully fit the idea of the funnel-like distribution model.[3,5,8,23,47,48]

The Chl-a's labeled as C706, C708 or C714 in PSI were experimentally identified as the low energy Chl-a (so-called red-Chls).[9,49–52] Exciton states of these experimentally assigned red-Chls need to be determined theoretically by considering short-range interactions. However, the putative 37th and 41th Chl-as do not belong to the previously identified candidates of red-Chls.[9,49–52] This may be due to the use of Poisson-TrESP/CDC methods that do not include the short-range electrostatic interactions as shown in Figure S5, in this study.

Correlation between the site energy values of each pair of counterpart pigments in hRC and PSI-core is shown in Figure 2, to see their function in the light-harvesting processes. PSI, in our numerical analysis, have two red-shifted Chl-a's of the 37th and 47th pigments. Their BChl-g counterparts in hRC, however, give positive values, as seen from Figure 2 and Table 1. On the other hand, 11th and 41th BChl-g's in hRC had more positive site energy shifts compared to that of P800, and their Chl-a counterparts in PSI had negative shifts compared to that of P700 (Figure 2). Homodimeric hRC and heterodimeric PSI, therefore, seem to give different electronic environments around these pigments. The difference suggests somewhat different paths/mechanisms of energy transfer in the two RCs because the overall correlation is virtually absent.

In Figure 1a, the excited state of 5(35)th pigment in the (second) lowest exciton state overlaps the excited states of 20(50)th and 28(58)th pigments coherently. The site energy shifts of these 5(35)th and 28(58)th pigments are negative as their counterparts Chl-a in PSI-core. The 28(58)th BChl-g has the site energy much lower than that of its counterpart Chl-a located nearby P700 in the PSI-core (Figure 3). We previously discussed the importance of 5(35)th BChl-g', which seems to connect the excited states between the upper and lower layers of BChl-g groups in hRC.[24] The 5(35)th BChl-g' mediates the excitation energy transfer from 11(41)th BChl-g to P800 in the downhill EET upon 770 nm photoexcitation. Consequently, the lowest exciton state over the 5(35)th, 20(50)th, and 28(58)th BChl-g seems to be functionally important in EET to P800 or in

dissipating the excess energy from the 28(58)th BCh-g to a carotenoid. In PSI, the carotenoids at these positions have been proposed to quench the triplet state of Chl-a too as the photoprotection mechanism.[53,54] Site-selective excitation of the carotenoid in this site, however, is experimentally difficult due to the existence of altogether 22 carotenoids in PSI. On the other hand, hRC contains only two in this symmetrical locations so that this carotenoid can be (site-selectively) exactly excited experimentally. This will facilitate functional studies of carotenoids in hRC and PSI.

The similarities in the arrangements and the site energy shift values of pigments between hRC and PSI, as typically seen for 5(35)th, 20(50)th, and 28(58)th BChl-g's, suggest common features in the two RCs. These pigments and their interactions with the surrounding protein environments, therefore, seem to be essential for the function of Type-I RCs.

We selected each pairs of pigments between hRC and PSI as listed in Table 1 based on the correlation rule as described in the Supporting Information. It is interesting that the pigments responsible for the lowest exciton state had the more negative site energy shifts compared to the other pigments in hRC and PSI, although the plot in Figure 2 apparently show rather weak correlation between PSI and hRC. It is also noted that the positions of the pigments forming the lowest exciton state of hRC are almost conserved in PSI and gRC.[19] The roles of amino acid residues surrounding these pigments in different RCs should be more carefully investigated in future studies.

CONCLUSION

We obtained the optical spectra of hRC by using the exciton Hamiltonian obtained by the structure-based calculations. It led to a comprehensive model that advances our preliminary models assuming the constant site energy shifts.[24] Excitonic couplings were calculated by Poisson-TrESP method and FED scheme, which have been well known in PSI, as done previously.[8,25] We calculated the site energy shift of each pigment in hRC in this study by the CDC method and analyzed the exciton dynamics in hRC. The absorption, CD and DAS spectra of hRC reproduced the experimental ones well. The spatial distribution of the site energy values and exciton states shown in Figures 1 and 3 showed that the site energies of a group of pigments nearby P800 are more negative forming a deep energy sink. The funnel model interprets this type of distribution of site energy shifts of BChl-g on hRC generally, and a group of pigments close to P800 are found to form energy sinks lower than the level of P800. It is also suggested that the carotenoids situated close to these pigments might work to dissipate the excess energy by transferring the triplet state of BChl-g into the carotenoid triplet state in the anaerobic organism. On the other hand, we could not find the counterparts of "putative red-shifted-Chl-a in PSI", which can be assumed to be 37th and 47th Chl-a's in PSI and have the very negative site energy shifts. BChl-g molecules at the counterpart locations in hRC show positive site energy shifts. PSI-core and hRC, therefore, have similar but not the same features as for the locations of pigments and the distribution pattern of site energy shifts (pigment-protein interaction) even with the low homology (less than 30%) between their protein amino acid sequences. PSI binds about 30 extra Chl-a's outside the core region, forms dimers and trimers of PSI, and binds multiple peripheral antenna complexes in contrast to hRC, which dimer or trimer states or extra antenna complex have not been known. The putative red-shifted-Chl-a sites in the PSI-core, whose counterparts in hRC have positive site energy shifts, therefore, might be developed to work as the energy sink to mediate EET from the peripheral pigments to P700, and/or work to trap and dissipate the extra excitation energy. The two RCs, which are probably originated from a common ancestral RC, thus, keep similar physicochemical light harvesting strategies but have been optimized differently. The hRC model developed here predicts that modifications of the key, low-exciton state, and pigment sites on hRC/PSI will produce significant alterations of their functions, and will give hints to understand their evolutionary relationship.

ACKNOWLEDGEMENTS

A.K. acknowledges support by a grant from KAKENHI (20K03880). H.K.-N. acknowledges support from JST, PRESTO grant number JPMJPR17G4. H.K.-N. and Y.S. acknowledge support from MEXT Quantum Leap Flagship Program (MEXT Q-LEAP), Grant Number JPMXS0120330644. S.I. acknowledges support by a grants from KAKENHI (17K07440 and 20K06684). The computation in this work has been partly done using the supercomputer of ACCMS, Kyoto University.

The authors are grateful to Drs. Hirozo Oh-oka of Osaka University and Chihiro Azai of Ritsumeikan University for their valuable discussions during the study.

Supporting Information Available

Dataset of the excitonic couplings used in the calculation. Graphical arrangements of the distribution probabilities of the excited state at BChl-g, BChl-g', and Chl-a_{F} in hRC for each exciton state from No. 1 to 60. Graphical representations of the distribution probabilities of the excited state at Chl-a in PSI for each exciton state from No. 1 to 96. Dataset of component decomposition of the site energy shift ($\epsilon_{\mathrm{eff}} = 1$) of hRC and PSI.

References

(1) Blankenship, R. E. *Molecular Mechanisms of Photosynthesis, 2nd Edition.*; John Wiley & Sons, Ltd.

(2) Sener, M. K.; Lu, D.; Ritz, T.; Park, S.; Fromme, P.; Schulten, K. Robustness and Optimality of Light Harvesting in Cyanobacterial Photosystem I. *J. Phys. Chem. B* **2002**, *106*, 7948–7960.

(3) Yang, M.; Damjanović, A.; Vaswani, H. M.; Fleming, G. R. Energy Transfer in Photosystem I of Cyanobacteria *Synechococcus elongatus*: Model Study with Structure-Based Semi-Empirical Hamiltonian and Experimental Spectral Density. *Biophys. J.* **2003**, *85*, 140 – 158.

(4) Heathcote, P.; Jones, M. R.; Fyfe, P. K. Type I Photosynthetic Reaction Centres: Structure and Function. *Phil. Trans. R. Soc. Lond. B* **2003**, *358*, 231–243.

(5) Vaitekonis, S.; Trinkunas, G.; Valkunas, L. Red Chlorophylls in the Exciton Model of Photosystem I. *Photosynth. Res.* **2005**, *86*, 185–201.

(6) Raszewski, G.; Renger, T. Light Harvesting in Photosystem II Core Complexes Is Limited by the Transfer to the Trap: Can the Core Complex Turn into a Photoprotective Mode? *J. Am. Chem. Soc.* **2008**, *130*, 4431–4446.

(7) Abramavicius, D.; Mukamel, S. Exciton Delocalization and Transport in Photosystem I of Cyanobacteria *Synechococcus elongates*: Simulation Study of Coherent Two-Dimensional Optical Signals. *J. Phys. Chem. B* **2009**, *113*, 6097–6108.

(8) Adolphs, J.; Müh, F.; Madjet, M. E.-A.; Busch, M. S. a.; Renger, T. Structure-Based Calculations of Optical Spectra of Photosystem I Suggest an Asymmetric Light-Harvesting Process. *J. Am. Chem. Soc.* **2010**, *132*, 3331–3343.

(9) Shibata, Y.; Yamagishi, A.; Kawamoto, S.; Noji, T.; Itoh, S. Kinetically Distinct Three Red Chlorophylls in Photosystem I of *Thermosynechococcus elongatus* Revealed by Femtosecond Time-Resolved Fluorescence Spectroscopy at 15 K. *J. Phys. Chem. B* **2010**, *114*, 2954–2963.

(10) Shibata, Y.; Nishi, S.; Kawakami, K.; Shen, J.-R.; Renger, T. Photosystem II Does Not Possess a Simple Excitation Energy Funnel: Time-Resolved Fluorescence Spectroscopy Meets Theory. *J. Am. Chem. Soc.* **2013**, *135*, 6903–6914.

(11) Kondo, T.; Matsuoka, M.; Azai, C.; Kobayashi, M.; Itoh, S.; Oh-oka, H. Light-Induced Electron Spin-Polarized (ESP) EPR Signal of the P800+ Menaquinone– Radical Pair State in Oriented Membranes of *Heliobacterium modesticaldum*: Role/Location of Menaquinone in the Homodimeric Type I Reaction Center. *J. Phys. Chem. B* **2018**, *122*, 2536–2543.

(12) Kato, K.; Shinoda, T.; Nagao, R.; Akimoto, S.; Suzuki, T.; Dohmae, N.; Chen, M.; Allakhverdiev, S. I.; Shen, J. R.; Akita, F. et al. Structural Basis for the Adaptation and Function of Chlorophyll f in Photosystem I. *Nat. Commun.* **2020**, *11*, 1–10.

(13) Kojima, R.; Yamamoto, H.; Azai, C.; Uragami, C.; Hashimoto, H.; Kosumi, D.; Oh-oka, H. Energy Transfer and Primary Charge Separation upon Selective Femtosecond Excitation at 810 nm in the Reaction Center Complex from Heliobacterium modesticaldum. *J. Photoch. Photobio. A* **2020**, *401*, 112758.

(14) Kondo, T.; Mutoh, R.; Tabe, H.; Kurisu, G.; Oh-Oka, H.; Fujiyoshi, S.; Matsushita, M. Cryogenic Single-Molecule Spectroscopy of the Primary Electron Acceptor in the Photosynthetic Reaction Center. *J. Phys. Chem. Lett.* **2020**, *11*, 3980–3986.

(15) Song, Y.; Sechrist, R.; Johnson, W.; Redding, K. E.; Ogilvie, J. P. Excitonic structure and charge transfer in the Heliobacterial Reaction Center probed by multispectral multidimensional spectroscopy. The 22nd International Conference on Ultrafast Phenomena 2020. 2020; p M2A.4.

(16) Gisriel, C.; Sarrou, I.; Ferlez, B.; Golbeck, J. H.; Redding, K. E.; Fromme, R. Structure of a Symmetric Photosynthetic Reaction Center–photosystem. *Science* **2017**, *357*, 1021–1025.

(17) Umena, Y.; Kawakami, K.; Shen, J.-R.; Kamiya, N. Crystal Structure of Oxygen-evolving Photosystem II at a Resolution of 1.9 Å. *Nature* **2011**, *473*, 55–61.

(18) Deisenhofer, J.; Epp, O.; Miki, K.; Huber, R.; Michel, H. X-ray Structure Analysis of a Membrane Protein Complex: Electron Density Map at 3 Å Resolution and a Model of the Chromophores of the Photosynthetic Reaction Center from Rhodopseudomonas viridis. *J. Mol. Biol.* **1984**, *180*, 385 – 398.

(19) Chen, J.-H.; Wu, H.; Xu, C.; Liu, X.-C.; Huang, Z.; Chang, S.; Wang, W.; Han, G.; Kuang, T.; Shen, J.-R. et al. Architecture of the photosynthetic complex from a green sulfur bacterium. *Science* **2020**, *370*.

(20) Oh-oka, H. Type 1 Reaction Center of Photosynthetic Heliobacteria † . *Photochem. Photobiol.* **2007**, *83*, 177–186.

(21) Hauska, G.; Schoedl, T.; Remigy, H.; Tsiotis, G. The Reaction Center of Green Sulfur Bacteria. *BBA* **2001**, *1507*, 260 – 277.

(22) Yu, L.-J.; Suga, M.; Wang-Otomo, Z.-Y.; Shen, J.-R. Structure of Photosynthetic LH1 – RC. *Nature* **2018**, *556*, 209–213.

(23) Jordan, P.; Fromme, P.; Witt, H. T.; Klukas, O.; Saenger, W.; Krauß, N. Three-Dimensional Structure of Cyanobacterial Photosystem I at 2.5 Å Resolution. *Nature* **2001**, *411*, 909–917.

(24) Kimura, A.; Itoh, S. Theoretical Model of Exciton States and Ultrafast Energy Transfer in Heliobacterial Type I Homodimeric Reaction Center. *J. Phys. Chem. B* **2018**, *122*, 11852–11859.

(25) Kitoh-Nishioka, H.; Shigeta, Y.; Itoh, S.; Kimura, A. Excitonic Coupling on a Heliobacterial Symmetrical Type-I Reaction Center: Comparison with Photosystem I. *J. Phys. Chem. B* **2020**, *124*, 389–403.

(26) Trost, J. T.; Blankenship, R. E. Isolation of a Photoactive Photosynthetic Reaction Center-core Antenna Complex from *Heliobacillus mobilis*. *Biochemistry* **1989**, *28*, 9898–9904.

(27) Neerken, S.; Aartsma, T. J.; Amesz, J. Pathways of Energy Transformation in Antenna Reaction Center Complexes of *Heliobacillus mobilis*. *Biochemistry* **2000**, *39*, 3297–3303.

(28) Liebl, U.; Lambry, J.-C.; Leibl, W.; Breton, J.; Martin, J.-L.; Vos, M. H. Energy and Electron Transfer upon Selective Femtosecond Excitation of Pigments in Membranes of *Heliobacillus mobilis*. *Biochemistry* **1996**, *35*, 9925–9934.

(29) Nuijs, A. M.; Dorssen, R. J. v.; Duysens, L. N. M.; Amesz, J. Excited States and Primary Photochemical Reactions in the Photosynthetic Bacterium *Heliobacterium chlorum*. *PNAS* **1985**, *82*, 6865–6868.

(30) Noort, P. I. V.; Gormin, D. A.; Aartsma, T. J.; Amesz, J. Energy Transfer and Primary Charge Separation in *Heliobacterium chlorum* Studied by Picosecond Time-resolved Transient Absorption Spectroscopy. *BBA-Bioenergetics* **1992**, *1140*, 15 – 21.

(31) Lin, S.; Chiou, H.; Kleinherenbrink, F.; Blankenship, R. Time-resolved Spectroscopy of Energy and Electron Transfer Processes in the Photosynthetic Bacterium *Heliobacillus mobilis*. *Biophys. J.* **1994**, *66*, 437 – 445.

(32) Francke, C.; Otte, S. C.; van der Heiden, J. C.; Amesz, J. Spurious Circular Dichroism Signals with Intact Cells of Heliobacteria. *BBA-Bioenergetics* **1994**, *1186*, 75 – 80.

(33) Hsu, C.-P.; You, Z.-Q.; Chen, H.-C. Characterization of the Short-Range Couplings in Excitation Energy Transfer. *J. Phys. Chem. C* **2008**, *112*, 1204–1212.

(34) Singh, U. C.; Kollman, P. A. An Approach to Computing Electrostatic Charges for Molecules. *J. Comput. Chem.* **1984**, *5*, 129–145.

(35) Maier, J. A.; Martinez, C.; Kasavajhala, K.; Wickstrom, L.; Hauser, K. E.; Simmerling, C. ff14SB: Improving the Accuracy of Protein Side Chain and Backbone Parameters from ff99SB. *J. Chem. Theory Comput.* **2015**, *11*, 3696–3713.

(36) Jorgensen, W. L.; Chandrasekhar, J.; Madura, J. D.; Impey, R. W.; Klein, M. L. Comparison of Simple Potential Functions for Simulating Liquid Water. *J. Chem. Phys.* **1983**, *79*, 926–935.

(37) Redfield, A. G. On the Theory of Relaxation Processes. *IBM J. Res. Dev.* **1957**, *1*, 19.

(38) Knox, R. S.; Spring, B. Q. Dipole Strengths in the Chlorophylls. *Photochem. Photobiol.* **2003**, *77*, 497–501.

(39) Pessarakli, M. E. *Handbook of Photosynthesis, Third Edition. Boca Raton*; CRC Press., 2016.

(40) Knutson, J. R.; Walbridge, D. G.; Brand, L. Decay-associated Fluorescence Spectra and the Heterogeneous Emission of Alcohol Dehydrogenase. *Biochemistry* **1982**, *21*, 4671–4679.

(41) Müh, F.; Lindorfer, D.; Schmidt Am Busch, M.; Renger, T. Towards a structure-based exciton Hamiltonian for the CP29 antenna of photosystem II. *Phys. Chem. Chem. Phys* **2014**, *16*, 11848–11863.

(42) Adolphs, J.; Müh, F.; Madjet, M. E. A.; Renger, T. Calculation of Pigment Transition Energies in the FMO Protein: From Simplicity to Complexity and Back. *Photosynth. Res.* **2008**, *95*, 197–209.

(43) Renger, T.; Marcus, R. A. On the Relation of Protein Dynamics and Exciton Relaxation in Pigment–protein Complexes: An Estimation of the Spectral Density and a Theory for the Calculation of Optical Spectra. *J. Chem. Phys.* **2002**, *116*, 9997–10019.

(44) Saito, S.; Higashi, M.; Fleming, G. R. Site-Dependent Fluctuations Optimize Electronic Energy Transfer in the Fenna–Matthews–Olson Protein. *J. Phys. Chem. B* **2019**, *123*, 9762–9772.

(45) Kim, Y.; Morozov, D.; Stadnytskyi, V.; Savikhin, S.; Slipchenko, L. V. Predictive First-Principles Modeling of a Photosynthetic Antenna Protein: The Fenna–Matthews–Olson Complex. *J. Phys. Chem. Lett.* **2020**, *11*, 1636–1643.

(46) Sumi, H. Theory on Rates of Excitation-Energy Transfer between Molecular Aggregates through Distributed Transition Dipoles with Application to the Antenna System in Bacterial Photosynthesis. *J. Phys. Chem. B* **1999**, *103*, 252–260.

(47) Damjanović, A.; Vaswani, H. M.; Fromme, P.; Fleming, G. R. Chlorophyll Excitations in Photosystem I of Synechococcus elongatus. *J. Phys. Chem. B* **2002**, *106*, 10251–10262.

(48) Brüggemann, B.; Sznee, K.; Novoderezhkin, V.; van Grondelle, R.; May, V. From Structure to Dynamics: Modeling Exciton Dynamics in the Photosynthetic Antenna PS1. *J. Phys. Chem. B* **2004**, *108*, 13536–13546.

(49) Rätsep, M.; Johnson, T. W.; Chitnis, P. R.; Small, G. J. The Red-Absorbing Chlorophyll a Antenna States of Photosystem I: A Hole-Burning Study of Synechocystis sp. PCC 6803 and Its Mutants. *J. Phys. Chem. B* **2000**, *104*, 836–847.

(50) Khmelnitskiy, A.; Toporik, H.; Mazor, Y.; Jankowiak, R. On the Red Antenna States of Photosystem I Mutants from Cyanobacteria Synechocystis PCC 6803. *J. Phys. Chem. B* **2020**, *124*, 8504–8515, PMID: 32852954.

(51) Riley, K. J.; Reinot, T.; Jankowiak, R.; Fromme, P.; Zazubovich, V. Red Antenna States of Photosystem I from Cyanobacteria Synechocystis PCC 6803 and Thermosynechococcus elongatus: Single-Complex Spectroscopy and Spectral Hole-Burning Study. *J. Phys. Chem. B* **2007**, *111*, 286–292, PMID: 17201451.

(52) Toporik, H.; Khmelnitskiy, A.; Dobson, Z.; Riddle, R.; Williams, D.; Lin, S.; Jankowiak, R.; Mazor, Y. The structure of a red-shifted photosystem I reveals a red site in the core antenna. *Nat. Commun.* **2020**, *11*, 5279.

(53) Cogdell, R. J.; Frank, H. A. How Carotenoids Function in Photosynthetic Bacteria. *Biochim. Biophys. Acta* **1987**, *895*, 63 – 79.

(54) Nilsson, R.; Merkel, P. B.; Kearns, D. R. Unambiguous Evidence For The Participation Of Singlet Oxygen ($^1\delta$) In Photodynamic Oxidation Of Amino Acids. *Photochem. Photobiol.* **1972**, *16*, 117–124.

Graphical TOC Entry